# Comparison of Cloud Properties from Ground-Based Infrared Cloud Measurement and Visual Observations

LEI LIU, XUE-JIN SUN, TAI-CHANG GAO, SHI-JUN ZHAO

*College of Meteorology and Oceanography, PLA University of Science and Technology, Nanjing, China*

(Manuscript received 6 August 2012, in final form 3 January 2013)

ABSTRACT

Cloud properties derived from the whole-sky infrared cloud-measuring system (WSIRCMS) are analyzed in relation to measurements of visual observations and a ceilometer during the period July–August 2010 at the Chinese Meteorological Administration Yangjiang Station, Guangdong Province, China. The comparison focuses on the performance and features of the WSIRCMS as a prototype instrument for automatic cloud observations. Cloud cover derived from the WSIRCMS cloud algorithm compares quite well with cloud cover derived from visual observations. Cloud cover differences between WSIRCMS and visual observations are within ±1 octa in 70.83% and within ±2 octa in 82.44% of the cases. For cloud-base height from WSIRCMS data and Vaisala ceilometer CL51, the comparison shows a generally good correspondence in the lower and midtroposphere up to the height of about 6 km, with some systematic difference due to different detection methods. Differences between the resulting cloud-type classifications derived from the WSIRCMS and from visual observations show that cumulus and cirrus are classified with high accuracy, but that stratocumulus and altocumulus are not. Stratocumulus and altocumulus are suggested to be treated as waveform cloud for classification purposes. In addition, it is considered an intractable problem for automatic cloud-measurement instruments to do cloud classification when the cloud amount is less than 2 octa.

## 1. Introduction

Clouds play an important role in the earth's radiation budget and climate change. Macroscopic cloud data such as cloud cover, cloud type, and cloud-base height (CBH) are traditionally observed by humans on the ground. Instrumentation for ground-based cloud measurements, such as ceilometers (Martucci et al. 2010), lidars (Wang and Sassen 2002), cloud radars (Atlas et al. 1995), microwave radiometers (Chan and Li 2009), and sky imagers (Shields et al. 1998; Long et al. 2006; Cazorla et al. 2008), have been developed and improved for years.

Presently, several countries, for example, Sweden, the United States, and the Netherlands, perform automated cloud observations using a ceilometer in combination with a cloud algorithm that transform ceilometer cloud-base readings at certain time intervals into cloud layers with corresponding amount and height. The automated cloud observations have been compared to visual observations. Studies (Perez et al. 2002; Wauben et al. 2006; Boers et al. 2010) show that the transition from human observers to instruments has resulted in unfortunate discontinuities in the time series of cloud observations that cannot be rectified a posteriori.

Some researchers suggest hemispheric instruments as the potential way to provide cloud properties in agreement with cloud observations. Algorithms for cloud detection and separation between clear-sky and cloudy conditions have been further improved to reduce uncertainties in deriving cloud cover and distribution (Shields et al. 1998; Long and Ackerman 2000; Pfister et al. 2003; Kassianov et al. 2005b; Huo and Lu 2009; Schade et al. 2009; Long 2010). Comparative analysis of whole-sky imager and visual observations was performed by Feister (2005) and Feister et al. (2010). They showed that the cloud cover differences are within ±1 octa in 65% and within ±2 octa in 79% of the cases studied. Schade et al. (2009) discussed the differences between the total cloud amounts derived from camera images and from human observations. The differences are within ±1 octa in 72% and within ±2 octa in 85% of the cases. However, visual camera systems only give

*Corresponding author address:* Lei Liu, College of Meteorology and Oceanography, PLA University of Science and Technology, No. 60 Shuanglong Street, Nanjing 211101, China.
E-mail: liuleidll@gmail.com

DOI: 10.1175/JTECH-D-12-00157.1

useful information during daytime and twilight, and they do not give information on the CBH, although stereoscopy using two wide-angled cameras makes it possible to obtain CBH (and wind) information (Seiz et al. 2002; Kassianov et al. 2005a).

Nowadays, the infrared camera systems are considered to have great potential to provide cloud cover, CBH, and cloud type, without any changes in performance during the day or the night (Shaw and Thurairajah 2003; Thurairajah 2004; Smith and Toumi 2008; Sun et al. 2008a, 2011b; Liu et al. 2011). Although these instruments are currently a little expensive to be considered for operational use, they have greater advantage compared with visual camera systems and some scanning infrared radiometers in continuous observation of both day and night with high-resolution images.

In this paper, we focus on the performance and results for the whole-sky infrared cloud-measuring system (WSIRCMS). It is a recently developed instrument that can obtain cloud cover, CBH, and cloud type. From July to August 2010, WSIRCMS, Vaisala ceilometer CL51, and human observations were performed at the Chinese Meteorological Administration (CMA) Yangjiang Station in southern Guangzhou Province, China. Previous studies (Feister 2005; Feister et al. 2010; Schade et al. 2009) mainly analyzed the differences between cloud cover derived from visible cloud imager and visual observations. In this paper, we systematically analyze cloud cover, CBH, and cloud-type measurement performance of WSIRCMS. The instruments that we used in the study are introduced in section 2. In section 3, cloud cover, CBH, and cloud-type determination algorithms for WSIRCMS are described. In section 4, cloud cover and cloud type derived from WSIRCMS and from visual observations are analyzed and compared. The differences between CBHs derived from WSIRCMS and from the ceilometer are also presented in section 4. A summary and conclusions are provided in section 5.

## 2. Instruments

The WSIRCMS and ceilometer CL51 were installed with a distance of 10 m between them on the rooftop of the Yangjiang observing station (21°50′N, 111°58′E; and 89.9 m above mean sea level). Visual cloud observations were performed with an observer standing in the middle of the two instruments on the hour from 0700 to 1800 local time (LT).

### a. WSIRCMS

The WSIRCMS is a ground-based passive sensor that uses an uncooled microbolometer detector array to measure downwelling atmospheric radiance in the 8–14-$\mu$m wavelength bands (Sun et al. 2008a,b; Sun 2009; Sun et al. 2009a, 2011a). It provides a way to obtain cloud distribution, calculate cloud amount, and estimate CBH, and to classify cloud types every 15 min with no difference in sensitivity during day and night for elevation angles greater than 15°. The primary WSIRCMS components are an optical detector, environmental parameter sensors, controller, power, and terminal unit. The optical detector is an uncooled microbolometer array containing 320 × 240 pixels. A whole-sky image is obtained under the control of the scan servo system after combining zenith image and other images at eight different orientations. The whole-sky image has a resolution of 650 × 650 pixels.

### b. Vaisala ceilometer CL51

Vaisala ceilometer CL51 employs pulsed diode laser lidar technology, where short, powerful laser pulses are sent out in a vertical or near-vertical direction (Vaisala 2012; Martucci et al. 2010). The laser is an InGasAs diode emitting at the 910-nm wavelength with a manufacturing estimated accuracy of ±5 m (against hard target) that is equal to the highest vertical resolution of $\Delta Z = 10$ m. Backscatter profiling is up to 15 km over full range. Its reporting cycle is programmable from 6 to 120 s. The resulting backscatter profile, that is, the signal strength versus the height, is stored and processed, and the cloud bases are detected. Knowing the speed of light, the time delay between the launch of the laser pulse and the detection of the backscatter signal indicates the CBH. Ceilometer CL51 is able to detect three cloud layers simultaneously.

## 3. Methods

### a. Algorithm used for cloud cover determination

The downward infrared radiance in 8–14 $\mu$m can be measured by WSIRCMS. If the measured radiance of a pixel is larger than the clear sky radiance, then the pixel can be determined as cloud. In clear sky, the downwelling infrared radiance in 8–14 $\mu$m varies with zenith angle, aerosol type and content, precipitable water vapor (PWV) content, etc. For a given aerosol type (rural aerosol type is used in this paper), visibility, and zenith angle, the relationship of downwelling infrared radiance $L$ and PWV can be expressed as Eq. (1) according to radiation transfer modeling results:

$$L = a \times \mathrm{PWV}^2 + b \times \mathrm{PWV} + c, \quad (1)$$

where coefficients $a$, $b$, and $c$ vary with visibility and zenith angle. We have calculated these coefficients using the Santa Barbara Discrete Ordinate (DISORT) Atmospheric

Radiative Transfer (SBDART) model for visibility at 1, 4, 10, and 23 km, with the elevation angle interval being 5°. From the simulated results, we can get the coefficients' lookup table (Sun 2009; Sun et al. 2011b).

It is known that vapor density logarithmically decreases with height. The vertical variation of vapor density with height may be written as

$$\rho z = \rho o \times \exp(-z/\mathrm{Hsc}), \tag{2}$$

where $\rho z$ is the vapor density at height $z$; $\rho o$ is the density of water vapor near the land surface; and Hsc is a constant, called the scale height that is defined as the altitude at which water vapor density falls to $1/e$ of the density near the land surface. According to Eq. (2), Hsc can be statistically calculated using historical radiosonde information. The value of the scale height is 1.93 km at our studied site from July to August.

Then, PWV can be calculated from the following equation:

$$\mathrm{PWV} = \rho o \times \mathrm{Hsc}/\rho_{\mathrm{H2O}}, \tag{3}$$

where $\rho_{\mathrm{H2O}}$ is density of liquid water.

The clear-sky radiance can be estimated from Eq. (1) according to real-time meteorological parameters, such as temperature, humidity, and visibility. Every pixel can be identified as cloud or clear sky based on the threshold method. The cloud cover can then be calculated.

### b. Algorithm used for CBH determination

The analysis of results of radiation transfer simulation shows a monotonic relationship between CBH and downwelling infrared radiation, which means for the same optical thickness of cloud, the higher the CBH is, the less the downwelling infrared radiation is received (Sun et al. 2012). In the case of known atmospheric conditions, we can calculate the downwelling infrared radiation of a certain height blackbody cloud layer using the SBDART model. The relationship of downwelling infrared radiance in this cloudy case and PWV can also be expressed as Eq. (1) according to radiation transfer modeling results. This is the basic principle of CBH remote sensing based on the use of downwelling infrared radiation.

Different CBHs can be chosen as appropriate boundary limit heights for fitting different latitudes. In the midlatitude, 2.5, 6, and 11 km can be chosen as appropriate boundary limit heights of the low-, mid-, and high-level clouds, respectively. Then, assuming that cloud radiates like a blackbody, the radiance for a cloud layer at the heights of 2.5, 6, and 11 km, which are recorded as $L_L$, $L_M$, and $L_H$, respectively, can be calculated by Eq. (1) with a given real-time PWV and precalculated coefficients $a$, $b$, and $c$. Radiation corresponding to the surface air temperature is denoted as $L_S$. Radiation measured by WSIRCMS is denoted as $L_r$. There is no cloud at this pixel if $L_r$ is less than $L_H$. In other conditions, the CBH can be calculated according to

$$H = \begin{cases} \dfrac{L_M - L_r}{L_M - L_H} \times (h_H - h_M) + h_M, & \text{when} \quad L_M > L_r \geq L_H \\ \dfrac{L_L - L_r}{L_L - L_M} \times (h_M - h_L) + h_L, & \text{when} \quad L_L > L_r \geq L_M \\ \dfrac{L_S - L_r}{L_S - L_L} \times h_L, & \text{when} \quad L_S > L_r \geq L_L \end{cases}, \tag{4}$$

where the values for $h_H$, $h_M$, and $h_L$ are 11, 6, and 2.5 km, respectively.

### c. Algorithm used for cloud-type classification

Cloud classification is a challenging task (Buch et al. 1995; Peura et al. 1996; Calbó and Sabburg 2008; Liu et al. 2011). Cloud type can be classified by sky condition classification combined with CBH.

We have studied ground-based cloud classification for several years (Sun et al. 2009b; Liu et al. 2011). Our experiments showed poor results when only the texture method was used to classify complex sky conditions. The accuracy is improved through the following algorithm:

The original infrared image is smoothed to suppress noise first. Then, it is enhanced using top-hat transformation and high-pass filtering. Top-hat transform (Soille 2003) is an operation that extracts small elements and details from given images. It is a residual filter that preserves the features in an image that can fit inside the structure element and removes those that cannot. Edges are detected from the enhanced image after adaptive optimization threshold segmentation and morphological edge detection. Several structural features are extracted from the segment image and edge image, such as cloud

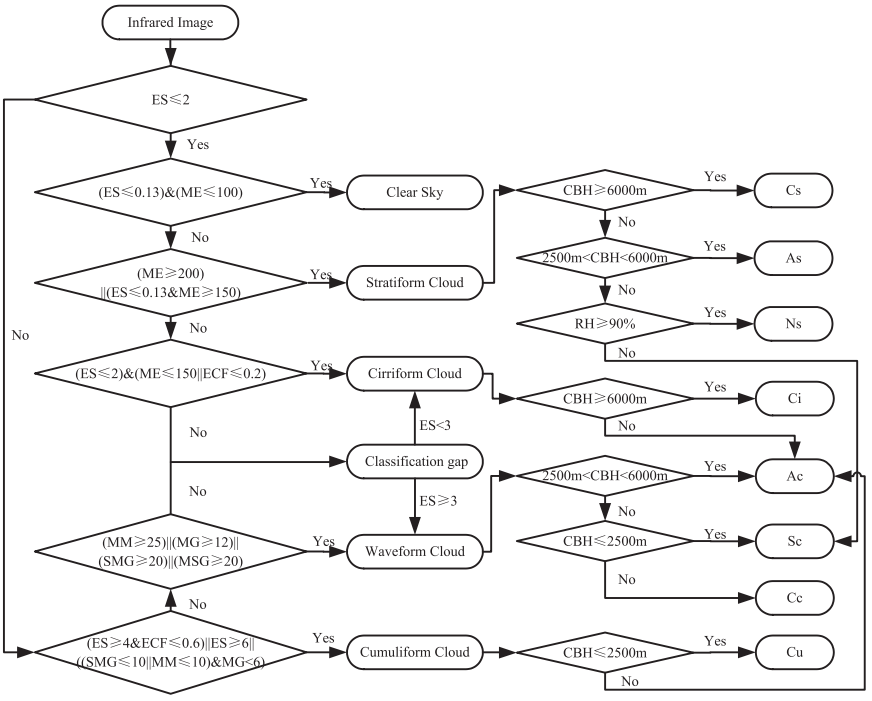


FIG. 1. Scheme illustrating the cloud-type classification, based on the threshold method.

gray mean value (ME), effective cloud fraction (ECF), edge sharpness (ES) and cloud mass and gaps distribution parameters including very small-sized cloud mass and gaps (SMG), mid-sized cloud gaps (MG), medium–small-sized cloud gaps (MSG), and main cloud mass (MM). Structural features descriptions were discussed in Liu et al. (2011). These features are different from common texture features by considering manual experiences, such as size, brightness, edge sharpness, and cloud size distribution information. They seem to be useful for ground-based cloud classification with images of high spatial resolution but for a relatively small area. The image is then classified into five different sky conditions: clear, cirriform clouds, stratiform clouds, waveform clouds, and cumuliform clouds using structural features with a simple but efficient supervised classifier called the rectangle method (Souza-Echer et al. 2006; Calbó and Sabburg 2008; Liu et al. 2011). After this process, the cloud type is classified by sky conditions combined with CBH. The flowchart is shown in Fig. 1.

## 4. Results and discussion

Atmospheric conditions during the comparison campaign were typical for summer, with upper-tropospheric temperatures above −70°C, and the integrated water vapor path derived from radiosonde data between 5 and 7 cm. In this study, we focus on the comparison between cloud data of the WSIRCMS and the site's macroscopic cloud data measured by ceilometer and visual observations. Since the observation time is different for each instrument, it is necessary to do time matching before comparisons to ensure consistency in time as closely as possible. Details are given in the following subsections.

### *a. Cloud cover comparison*

Cloud cover results from WSIRCMS are compared to visual observations to define the quality of the retrieval methods. The visual observations were made on the hour during daytime, while the WSIRCMS obtained cloud cover every 15 min day and night. Thus, the results from WSIRCMS are taken as closely as possible to the visual observation time.

Data derived from WSIRCMS and visual observations were multiplied by 0.8 and rounded to the nearest integer in order to convert cloud cover from tenths to octas. For comparison, we choose the same score index as defined by Dürr and Philipona (2004), namely,

$$\text{Score} = 100 \times \frac{n[\pm 1(2)\text{octa}]}{n}\%, \qquad (5)$$

where $n[\pm 1(2)$ octa$]$ are cases with a maximum difference of 1(2) octa between WSIRCMS and observations, and $n$ is the number of cases.

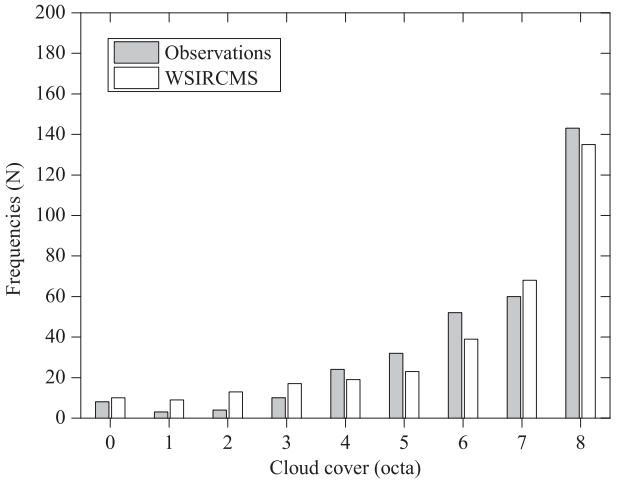


FIG. 2. Frequency distribution of the cloud covers from WSIRCMS and visual observations in the period July–August 2010 at the CMA Yangjiang Station.

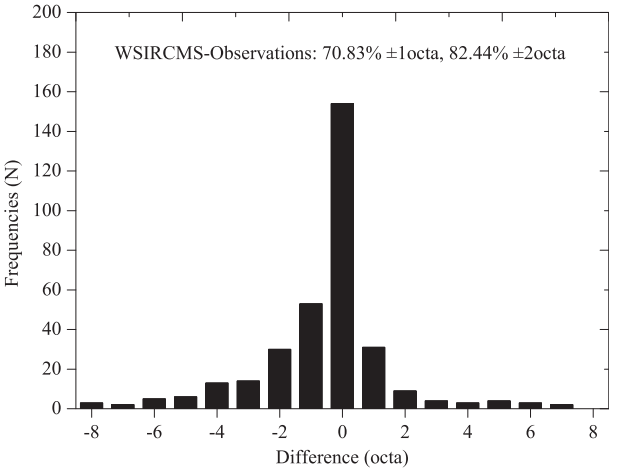


FIG. 3. Frequency distribution of the differences in cloud covers between WSIRCMS and visual observations in the period July–August 2010 at the CMA Yangjiang Station.

The occurrences of detected cloud cover from WSIRCMS and visual observations datasets of 9-octa bins are shown in Fig. 2. It indicates good agreement between visual observations and WSIRCMS. Basically, results from WSIRCMS are higher than visual observations at smaller cloud cover, while results from WSIRCMS are lower at larger cloud cover.

The frequency plot of differences between total cloud cover from WSIRCMS and visual observations are shown in Fig. 3. The deviations are nearly symmetrically distributed around zero. The mean difference (overall bias) is merely −0.3 octa, the mean cloud amount for the visual observation is 6.7 octa, while that for the WSIRCMS is 6.4 octa. More than 70% of the differences are within ±1 octa, which is the estimated uncertainty of cloud cover observations, and about 82% of the differences are within ±2 octa. There are large differences up to −8 and +7 octa in some cirrus clouds cases. The misinterpretation of the WSIRCMS is most likely due to the error of clear-sky threshold caused by PWV estimation.

### *b. Cloud-base-height comparison*

The ceilometer CL51 used in this study is a zenith-pointing measurement, which can detect three cloud layers simultaneously every 36 s. The WSIRCMS can provide CBH for an elevation angle greater than 15° every 15 min. And, CBH at different levels can also be estimated. For comparison, we choose the lowest height for zenith angles less than 5° as the CBH at zenith detected by WSIRCMS. The minimum height of the lowest cloud layer within 2 min around the WSIRCMS's observation time is chosen as the CBH at zenith obtained by ceilometer CL51.

CBH values for the period 0000–2359 LT 28 July 2010 from the two instruments are shown as an example in Fig. 4. In general, CBHs from WSIRCMS and the active sounder CL51 show a close correspondence with low-level clouds, though a few unacceptably large differences remain.

Data with large differences are carefully analyzed. First, some obvious low-level broken clouds seen in the WSIRCMS images were not detected by ceilometer or mistakenly detected as high clouds. This is mainly due to the received laser signals from the cloud gaps. Second, the ceilometer did not identify part of the high and thin cirrus clouds that scattered insufficient radiation to cause a detectable signal. Third, a small part of the homogeneous cloud seen in the WSIRCMS image and by

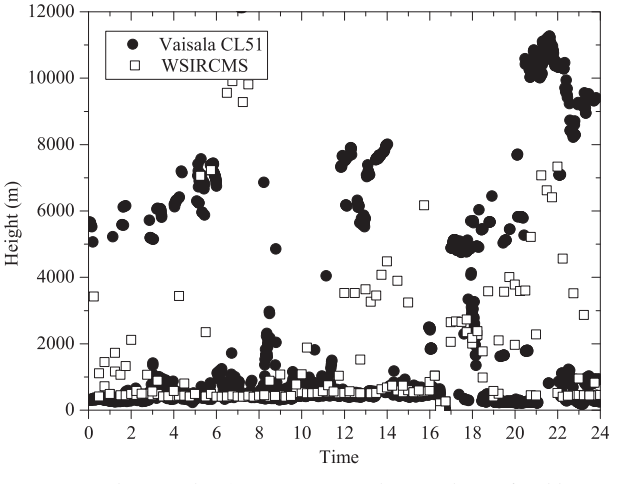


FIG. 4. The 28 Jul 2010 case: CBH values as determined by WSIRCMS and Vaisala CL51.

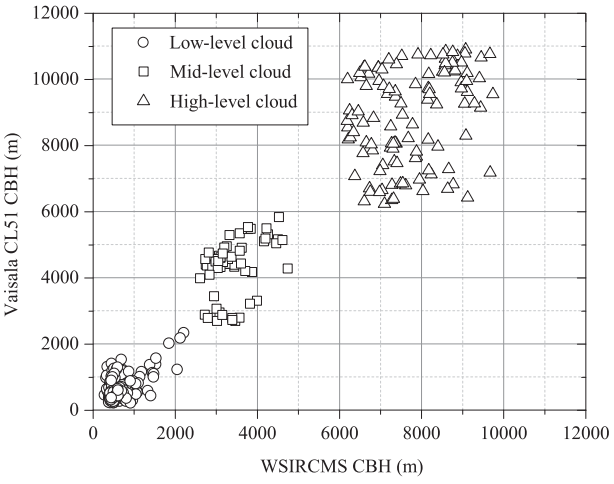


FIG. 5. CBHs from WSIRCMS compared to CBH from the ceilometer during the period July–August 2010 at the CMA Yangjiang Station.

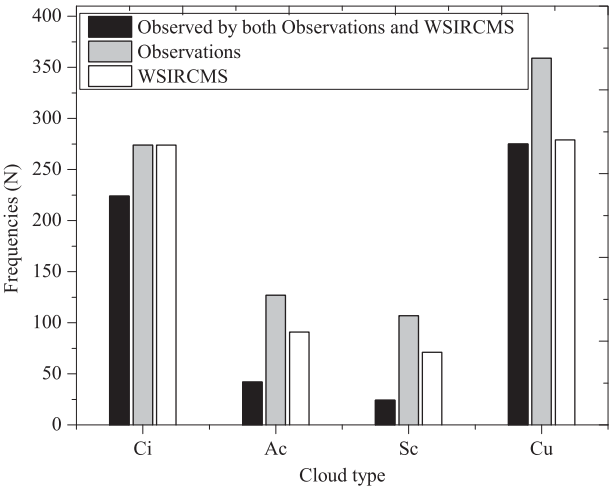


FIG. 6. Frequency distribution of the cloud types from WSIRCMS and visual observations during the period July–August 2010 at the CMA Yangjiang Station.

observers was not detected by the ceilometer if there was much haze in the atmosphere. Last, the ceilometer detected some clouds that were not seen by the WSIRCMS image or the observer. This situation was found and discussed by Feister et al. (2010). It presumably happens when a transparent vapor level exists in the upper air and causes an elusive cloud signal. Such data are excluded from those used for comparison between WSIRCMS and ceilometer CL51. A total of 417 data pairs are retained with 242 low-level clouds, 114 midlevel clouds, and 61 high-level clouds for further analysis.

After the screening of the data, the CBH differences between WSIRCMS and the ceilometer for the whole dataset can be seen in the scatterplot of Fig. 5. It shows a closer correspondence with smaller scatter for low-level clouds; their mean absolute difference is 227 m, with the standard deviation being 218 m. Systematic differences are more pronounced between the two instruments for midlevel clouds; their mean absolute difference is 1123 m, with the standard deviation being 530 m. High differences can be seen at high-level clouds; their mean absolute difference is 1610 m, with the standard deviation being 1056 m. It can be seen that, with increasing cloud-base height, the difference of the results measured by the two devices becomes greater, especially for high-level clouds. The main reason is that we assume that all types of clouds are blackbody. However, high-level clouds should not be treated as blackbody. Therefore, we believe that the above-mentioned method in this study is effective for low-level and midlevel clouds, but for the high-level clouds the method is for reference only.

### c. *Cloud-type comparison*

Yangjiang is of tropical climate with few cloud-type variety [cumulus (Cu), stratocumulus (Sc), cumulonimbus (Cb), altocumulus (Ac), and cirrus (Ci), etc.] during summer days. The classification of Cb will not be discussed here because it cannot be identified by WSIRCMS without the atmospheric electric field measurement. Each image can be classified into more than one cloud type, by both the WSIRCMS and observers. The occurrences of detected cloud type from WSIRCMS and visual observations datasets are shown in Fig. 6. It indicates that the frequencies in each cloud type detected by WSIRCMS are smaller than those from visual observations. In addition, Cu and Ci derived from WSIRCMS show good agreement with visual observation data (the accuracy is 81.8% and 76.6%, respectively), but Ac and Sc do not (the accuracy is only 33.1% and 22.4%, respectively). Cloud type with a small cloud amount can be easily detected by human eyes, while it is difficult for instruments. This is the possible reason that can be used to explain the classification differences between instruments and observers. The agreement between WSIRCMS and observers for cloud type with different cloud amount is shown in Table 1. Note that we do not take into account the ''clear'' sky class, which is the most unpopular during the experience time.

It seems that cloud classification ability of the instrument is good when cloud amount is no lower than 2 octa, especially for Cu and Ci, with the indices of agreement (accuracy) being 88.7% and 84.9%, respectively. But the agreement of Ac and Sc is not high (below 50%). Since ''confusions'' can often be found between Ac

TABLE 1. The agreement between WSIRCMS and observer for cloud types with different cloud amounts during the period July–August 2010 at the CMA Yangjiang Station. For different cloud amounts of four cloud types, the numbers of each cloud type derived from observer [*N*(Observer)] are treated as the truth. The WSIRCMS-derived cloud-type accuracy means *N*(WSIRCMS)/*N*(Observer) × 100%.

| | | ≥1 octa | ≥2 octa | ≥3 octa | ≥4 octa | ≥5 octa |
|---|---|---|---|---|---|---|
| Ci | Observer | 274 | 203 | 117 | 96 | 64 |
| | WSIRCMS | 224 | 180 | 108 | 89 | 60 |
| | Accuracy (%) | 81.8 | 88.7 | 92.3 | 92.7 | 93.8 |
| Ac | Observer | 127 | 55 | 25 | 14 | 8 |
| | WSIRCMS | 42 | 25 | 12 | 6 | 5 |
| | Accuracy (%) | 33.1 | 45.5 | 48.0 | 42.9 | 62.5 |
| Sc | Observer | 107 | 54 | 28 | 23 | 16 |
| | WSIRCMS | 24 | 16 | 13 | 11 | 8 |
| | Accuracy (%) | 22.4 | 29.6 | 46.4 | 47.8 | 50.0 |
| Cu | Observer | 359 | 292 | 180 | 130 | 97 |
| | WSIRCMS | 275 | 248 | 171 | 125 | 92 |
| | Accuracy (%) | 76.6 | 84.9 | 95.0 | 96.2 | 94.8 |

and Sc, in Table 2 we show a new contingency matrix where these two classes are accounted as one type, defined as waveform cloud. Then, the accuracy index becomes 78.0% for a cloud amount no less than 2 octa, which shows a good agreement for waveform cloud.

From a detailed analysis of Tables 1 and 2, it becomes apparent that confusions on waveform cloud (Ac and Sc) with cloud amount less than 2 octa are more common than with other types of clouds (say, Cu and Ci). After checking these misclassified images, we find that most of them were stratocumulus cumulogenitus and altocumulus cumulogenitus, whose wavy structures are not shown completely but puffy in appearance, similar to cotton balls. Therefore, we understand why these images produced values for features similar to cumuliform clouds.

Further discussion on the disagreement of data shows that several images that should be classified as Ac and Cu (according to visual inspection) are automatically classified as Sc and Cu. This usually happens when a certain amount of Cu cloud and Ac cloud appeared just above Cu, resulting in large cloud fraction overlaps. Infrared radiation obtained by instrument is a stack of cloud and sky background radiation, and it is difficult for WSIRCMS to distinguish whether large infrared radiation is caused by Sc or by Ac plus Cu. Probably this confusion could be resolved by using other methods, for example, using multiscale geometric analysis (MGA) technology (Romberg et al. 2003), which means the original cloud image could be analyzed under a family of scale spaces, just like human beings.

Also, there are some images that were visually identified as Sc but classified as Cu. After checking these images, we find that in these images Sc with a cloud amount less than 5 octa is at the edge of the image, which means these clouds were at low elevation angles. This is attributed to the ''packing effect,'' a condition where clouds near the horizon appear to blend together or overlap due to the viewing angle. The origin of this problem is a well-known issue, namely, the ''perspective effect'' of the sky in the horizon of the sky dome. This problem is difficult to solve.

TABLE 2. The agreement between WSIRCMS and observer for waveform cloud (Ac and Sc accounted together in this paper) with different cloud amounts.

| | ≥1 octa | ≥2 octa | ≥3 octa | ≥4 octa | ≥5 octa |
|---|---|---|---|---|---|
| Observer | 234 | 109 | 53 | 37 | 24 |
| WSIRCMS | 130 | 85 | 41 | 29 | 19 |
| Accuracy (%) | 55.6 | 78.0 | 77.4 | 78.4 | 79.2 |

Finally, some images that corresponded to overcast skies (observed as Ac) were classified as Sc, or Sc classified as Ac. We checked these images very carefully, and tried to use CBH data from ceilometer CL51 to confirm these cloud types. It is found that this complexion may be due to the uncertainty of human observations. As for an explanation, we chose data on 21 July 2010. During that day, Typhoon Chanthu affected the Yangjiang area, and made a landfall along the Wuchuan coast in Guangdong Province at 1345 LT 22 July. Figure 7 shows the CBH obtained by ceilometer CL51 and WSIRCMS. It seems that the clouds constantly became thicker and lower. CBH from WSIRCMS was lower than that from the ceilometer, and the decline trend was more pronounced for WSIRCMS. Cloud types classified by observers were all Sc from 0700 to 1900 LT.

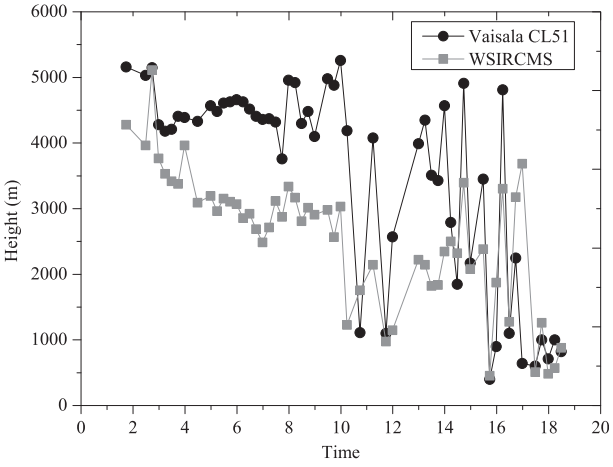


FIG. 7. The 21 Jul 2010 case: CBH values as determined by WSIRCMS and Vaisala CL51.

But from 0700 to 0900 LT, the CBH was higher than 2500 m from both WSIRCMS and ceilometer CL51, which means the cloud could also be classified as Ac. This usually happens when the visibility is not good or the CBHs are limited in the ranges of 2000–3000 m. In fact, cloud can be classified as either Ac or Sc in this height range. Therefore, we suggest Ac and Sc be treated as waveform cloud, when classified by automatic cloud-measurement instruments.

## 5. Conclusions

This paper compares cloud cover, CBH, and cloud type derived from WSIRCMS with estimates from visual observations and a ceilometer at the CMA Yangjiang Station, Guangdong Province, China. The performance of WSIRCMS-derived cloud properties is analyzed with caution.

Cloud cover comparisons are carried out between WSIRCMS and visual observations. Only slight systematic differences have been found between the WSIRCMS and visual observations. The WSIRCMS-based skill score is 70.83% (82.44%) at ±1 (2)-octa tolerance. This result shows the consistency of WSIRCMS and whole-sky visible imager mentioned in other studies (Feister and Shields 2005; Feister et al. 2010; Schade et al. 2009) in the performance of cloud cover measurement. In addition, it can provide cloud properties with no difference in sensitivity during day and night. Therefore, WSIRCMS is a possible candidate replacement for the visual observations.

Referring to CBHs, the comparison shows reasonable agreement between WSIRCMS and ceilometers, especially for height levels less than 3 km. There are larger differences for midlevel and high-level clouds than for lower-level clouds. CBH differences between the two instruments are mainly due to different measurement principles and the definition of CBH for the respective instrument. Moreover, both instruments may have some measurement errors; a combination of the two instruments should be investigated later.

Some cloud types (say, Cu and Ci) derived from WSIRCMS show good agreement with visual observation data, but others (say, Ac and Sc) are not. We suggest Ac and Sc be treated as waveform cloud to be classified by instruments. In addition, we consider that for cloud-measurement instruments, there is a knotty issue on cloud classification when the cloud amount is less than 2 octa. Perhaps, we do not need to pay great attention to cloud classification problems caused by a small amount of clouds. A test using a numerical model might help to determine the impact of such a small amount of clouds for different cloud types on a weather system or a regional climate.

*Acknowledgments.* This research was jointly supported by the National Natural Science Foundation of China (Grant 41205125) and the public benefit sector of China [Grant GYHY(QX)200806030,201306068]. The authors thank the staff and data providers at the Chinese Meteorological Administration (CMA) Yangjiang Station for their assistance. We also acknowledge the CMA Meteorological Observation Center for their support to improve the measurements of cloud parameters.

## REFERENCES

Atlas, D., S. Y. Matrosov, A. J. Heymsfield, M.-D. Chou, and D. B. Wolff, 1995: Radar and radiation properties of ice clouds. *J. Appl. Meteor.,* **34,** 2329–2345.

Boers, R., M. de Haij, W. M. F. Wauben, H. Klein Baltink, L. H. van Ulft, M. Savenije, and C. N. Long, 2010: Optimized fractional cloudiness determination from five ground-based remote sensing techniques. *J. Geophys. Res.,* **115** (D24), D24116, doi:10.1029/2010JD014661.

Buch, K. A., C.-H. Sun, and L. R. Thorne, 1995: Cloud classification using whole-sky imager data. *Proc. Fifth Atmospheric Radiation Measurement (ARM) Science Team Meeting,* San Diego, CA, U.S. Department of Energy, 35–39.

Calbó, J., and J. Sabburg, 2008: Feature extraction from whole-sky ground-based images for cloud-type recognition. *J. Atmos. Oceanic Technol.,* **25,** 3–14.

Cazorla, A., J. Olmo, and L. Alados-Arboledas, 2008: Development of a sky imager for cloud cover assessment. *J. Opt. Soc. Amer.,* **25A,** 29–39.

Chan, P. W., and C. M. Li, 2009: Comparison of total cloud amount determined by a ceilometer and a microwave radiometer. *Proc. Eighth Int. Symp. on Tropospheric Profiling: Integration of Needs, Technologies and Applications,* Delft, Netherlands, 4 pp. [Available online at http://www.hko.gov.hk/publica/reprint/r851.pdf.]

Dürr, B., and R. Philipona, 2004: Automatic cloud amount detection by surface longwave downward radiation measurements. *J. Geophys. Res.,* **109,** D05201, doi:10.1029/2003JD004182.

Feister, U., and J. Shields, 2005: Cloud and radiance measurements with the VIS/NIR daylight whole sky imager at Lindenberg (Germany). *Meteor. Z.,* **14,** 627–639.

——, H. Möller, T. Sattler, J. Shields, U. Görsdorf, and J. Güldner, 2010: Comparison of macroscopic cloud data from ground-based measurements using VIS/NIR and IR instruments at Lindenberg, Germany. *Atmos. Res.,* **96,** 395–407.

Huo, J., and D. R. Lu, 2009: Cloud determination of all-sky images under low-visibility conditions. *J. Atmos. Oceanic Technol.,* **26,** 2172–2181.

Kassianov, E., C. N. Long, and J. Christy, 2005a: Cloud-base-height estimation from paired ground-based hemispherical observations. *J. Appl. Meteor.,* **44,** 1221–1233.

——, ——, and M. Ovtchinnikov, 2005b: Cloud sky cover versus cloud fraction: Whole-sky simulations and observations. *J. Appl. Meteor.,* **44,** 86–98.

Liu, L., X. J. Sun, F. Chen, S. J. Zhao, and T. C. Gao, 2011: Cloud classification based on structure features of infrared images. *J. Atmos. Oceanic Technol.,* **28,** 410–417.

Long, C. N., 2010: Correcting for circumsolar and near-horizon errors in sky cover retrievals from sky images. *Open Atmos. Sci. J.,* **4,** 45–52.

——, and T. P. Ackerman, 2000: Identification of clear skies from broadband pyranometer measurements and calculation of downwelling shortwave cloud effects. *J. Geophys. Res.,* **105** (D12), 15 609–15 626.

——, J. Sabburg, J. Calbó, and D. Pageś, 2006: Retrieving cloud characteristics from ground-based daytime color all-sky images. *J. Atmos. Oceanic Technol.,* **23,** 633–652.

Martucci, G., C. Milroy, and C. D.Ö. Dowd, 2010: Detection of cloud-base height using Jenoptik CHM15K and Vaisala CL31 ceilometers. *J. Atmos. Oceanic Technol.,* **27,** 305–318.

Perez, R., J. A. Bonaventura-Sparagna, M. Kmiecik, R. George, and D. Renné, 2002: Indications of biases in reporting cloud cover at major airports. *Sixth Symp. on Integrated Observing Systems,* Orlando, FL, P1.1. [Available online at https://ams.confex.com/ams/pdfpapers/28467.pdf.]

Peura, M., A. Visa, and P. Kostamo, 1996: A new approach to land based cloud classification. *Proc. 13th Int. Conf. on Pattern Recognition (ICPR'96),* Vienna, Austria, IEEE Computer Society Press, 143–147.

Pfister, G., R. L. McKenzie, J. B. Liley, A. Thomas, B. W. Forgan, and C. N. Long, 2003: Cloud coverage based on all-sky imaging and its impact on surface solar irradiance. *J. Appl. Meteor.,* **42,** 1421–1434.

Romberg, J. K., M. B. Wakin, and R. G. Baraniuk, 2003: Multiscale geometric image processing. *Visual Communication Image Processing 2003,* T. Ebrahimi and T. Sikora, Eds., International Society for Optical Engineering (SPIE Proceedings, Vol. 5150), 1265–1272, doi: 10.1117/12.509903.

Schade, N. H., A. Macke, H. Sandmann, and C. Stick, 2009: Total and partial cloud amount detection during summer 2005 at Westerland (Sylt, Germany). *Atmos. Chem. Phys.,* **9,** 1143–1150.

Seiz, G., E. P. Baltsavias, and A. Gruen, 2002: Cloud mapping from the ground: Use of photogrammetric methods. *Photogramm. Eng. Remote Sens.,* **68,** 941–951.

Shaw, J. A., and B. Thurairajah, 2003: Short-term Arctic cloud statistics at NSA from the infrared cloud imager. *Proc. 13th Atmospheric Radiation Measurement (ARM) Science Team Meeting,* Broomfield, CO, ARM, 7 pp. [Available online at http://www.arm.gov/publications/proceedings/conf13/extended_abs/shaw-ja.pdf.]

Shields, J. E., M. E. Karr, T. P. Tooman, D. H. Sowle, and S. T. Moore, 1998: The whole sky imager—A year of progress. *Proc. Eighth Atmospheric Radiation Measurement (ARM) Science Team Meeting,* Tucson, AZ, ARM, 9 pp. [Available online at http://www.mpl.ucsd.edu/people/jshields/publications/wsi.progress.pdf.]

Smith, S., and R. Toumi, 2008: Measuring cloud cover and brightness temperature with a ground-based thermal infrared camera. *J. Appl. Meteor. Climatol.,* **47,** 683–693.

Soille, P., 2003: *Morphological Image Analysis: Principles and Applications.* 2nd ed. Springer-Verlag, 391 pp.

Souza-Echer, M. P., E. B. Pereira, L. S. Bins, and M. A. R. Andrade, 2006: A simple method for the assessment of the cloud cover state in high-latitude regions by a ground-based digital camera. *J. Atmos. Oceanic Technol.,* **23,** 437–447.

Sun, X. J., 2009: Study on the ground-based infrared remote sensing of whole sky cloud (in Chinese). Ph.D. thesis, Institute of Physics, Beijing University, 145 pp.

——, T. C. Gao, D. L. Zhai, S. J. Zhao, and J. G. Lian, 2008a: Whole sky infrared cloud measuring system based on the uncooled infrared focal plane array (in Chinese). *Infrared Laser Eng.,* **37,** 761–764.

——, J. Liu, S. J. Zhao, D. L. Zhai, and J. T. Mao, 2008b: Radiometric calibration model of the uncooled infrared focal plane array (in Chinese). *J. PLA Univ. Sci. Technol.,* **9,** 399–403.

——, ——, and J. T. Mao, 2009a: Vicarious calibration on the sensor of whole sky infrared cloud measuring system (in Chinese). *J. Infrared Millimeter Waves,* **28,** 54–57.

——, L. Liu, T. C. Gao, S. J. Zhao, J. Liu, and J. T. Mao, 2009b: Cloud classification of the whole sky infrared image based on the fuzzy uncertainty texture spectrum (in Chinese). *J. Chin. Appl. Meteor. Sci.,* **20,** 157–163.

——, F. Chen, L. Liu, Y. N. Hu, and S. J. Zhao, 2011a: Cloud identification combining threshold with texture (in Chinese). *J. PLA Univ. Sci. Technol.,* **12,** 397–402.

——, L. Liu, and S. J. Zhao, 2011b: Whole sky infrared remote sensing of cloud. *Procedia Earth Planet. Sci.,* **2,** 278–283.

——, C. Qin, J. Qin, L. Liu, and Y. N. Hu, 2012: Ground-based infrared remote sensing based on the height of middle and low cloud (in Chinese). *J. Remote Sens.,* **16,** 166–173.

Thurairajah, B., 2004: Thermal infrared imaging of the atmosphere: The infrared cloud imager. M.S. thesis, Dept. of Electrical and Computer Engineering, Montana State University, 110 pp. [Available online at http://etd.lib.montana.edu/etd/2004/thurairajah/ThurairajahB04.pdf.]

Vaisala, cited 2012: Vaisala ceilometer CL51. [Available online at http://www.vaisala.com/en/products/ceilometers/Pages/CL51.aspx.]

Wang, Z., and K. Sassen, 2002: Cirrus cloud microphysical property retrieval using lidar and radar measurements. Part I: Algorithm description and comparisons with in situ data. *J. Appl. Meteor.,* **41,** 218–229.

Wauben, W. M. F., H. Klein Baltink, M. de Haij, N. Maat, and J. Verkaik, 2006: Status, evaluation and new developments in the automated cloud observations in the Netherlands. *Proc. WMO Tech. Conf. on Meteorological and Environmental Instruments and Methods of Observation (TECO-2006),* Geneva, Switzerland, WMO, 10 pp. [Available online at http://www.wmo.int/pages/prog/www/IMOP/publications/IOM-94-TECO2006/1(7)_Wauben_Netherlands.pdf.]